Potential of compositional complex oxide in reversible electrochemical energy storage

Shaw Su

A thesis
submitted in partial fulfillment of the
requirements for the degree of

Master of Science

University of Washington
2022

Committee:
Guozhong Cao
Dwayne Arola

Program Authorized to Offer Degree:
Material Science and Engineering

University of Washington

Abstract

Potential of compositional complex oxide in reversible electrochemical energy storage

Shaw Su

Chair of the Supervisory Committee:
Guozhong Cao
Material Science and Engineering

Compositional complex or high entropy materials, due to their unique phase stabilization mechanism, have ushered exciting research opportunities for material property design on many fronts, and perhaps more importantly, given rise to prospect of developing fundamental understanding of complex material systems whereby material functions may be tailored to fit various application needs simultaneously.

In the area of electrochemical energy storage, high entropy materials have shown promising results both in storage capacity and longevity in lithium ion batteries owing to their efficient conversion type reaction mechanism, which can pave the way for more sustainable energy storage in the near future. Moreover, high entropy materials tend to retain structural integrity more than traditional binary or ternary metal complex and show interesting results insofar as the attributes of constituents, which can range from mechanical to electronic properties, may be aggregated and manifested in a single combined phase, and in some cases the single combined phase is imparted with superior attributes than the phase mixture of aggregated whole. Research into the underpinnings of this phenomenon can enable design of complex

material systems with potential to address many challenges faced in the broader community today.

A compositional complex oxide $(V_{0.25}Mn_{0.25}Fe_{0.25}Co_{0.25})_{1-x}Ni_xO$ was synthesized and characterized in this paper. Its structural properties entailed a mixture a primary spinel and secondary triclinic phases crystallized in predominantly nanometer sized grains with near equimolar composition of transition metals sans nickel. Elemental composition was in uniform distribution, and oxidation states were multi-valent. Cyclic voltammetry, galvanostatic and electrochemical impedance data altogether concur and support for a conversion type reaction consisted of equally fast surface kinetic and long range diffusion, with high probability of entropic stabilization. The findings show convincing connection between structural and compositional material properties and electrochemical responses. Further studies are necessary to shed light on the pertaining fundamentals.

Contents

1. Introduction

Volatility in oil price in conjunction with deteriorating environmental metrics, both of which exacerbated by the exponential population growth the world saw in the last half-century, are pushing alternative energy sources to instill sustainability in the global supply chain. Rising energy demand at home as evident in Figure 1 necessitated the shift to energy sources with high energy density and low adverse impacts, which has in so doing propelled growths of renewables, nuclear, and natural gas in energy production. [1] Electric energy production shown in Figure 2 accounts for approximately 35.7 quads (quadrillion British thermal units), or 38% of all energy consumed in 2020, albeit at the efficiency of 35%, which indicates not only significant energy loss but also opportunity to store excess energy as auxiliary for spikes or irregularities in the electric grid. [1] Moreover, in place and proposed sustainable energy initiatives are expected to electrify the transportation sector with estimated annual growth rate of over 20% in the coming decade,[2] which sets the stage for breakthroughs in energy storage research to address challenges pertaining to capacity, longevity and safety faced in the electric vehicle market today.

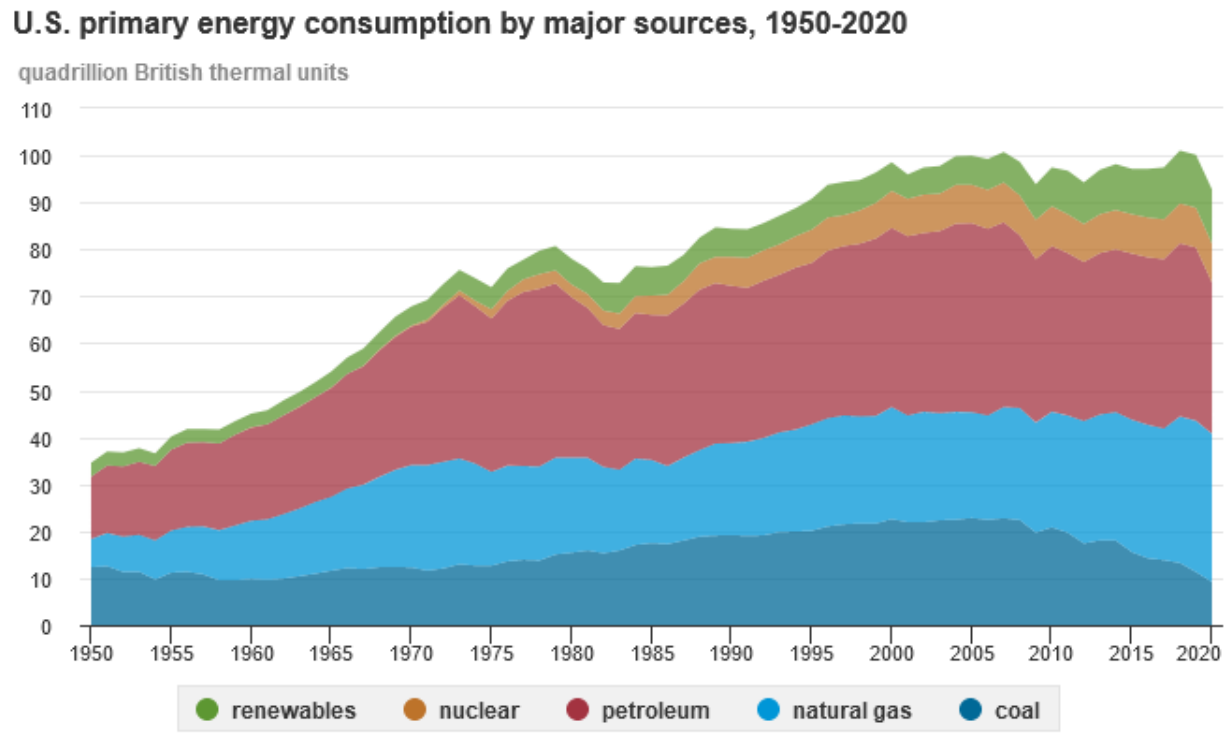

Figure 1 Domestic energy consumption by source from 1950-2020, renewable sources include biomass, wind, hydroelectric, solar, and geothermal. [1]

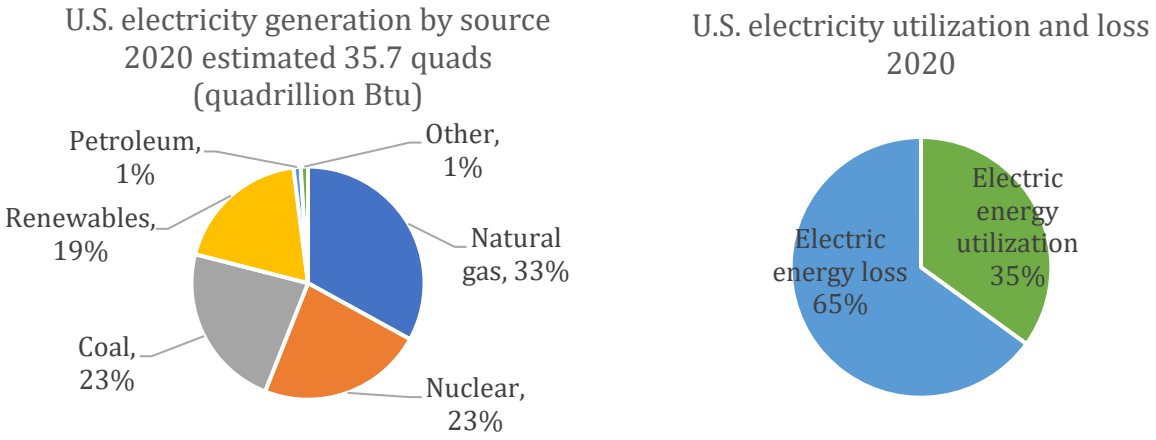

Figure 2 Breakdown of 2020 domestic electric energy production by source as well as electricity utilization efficiency. [1]

At the center of energy storage lay materials with which storage chemistry is entailed, and for batteries, which are the primary conduit for storing electric charges with high energy density, stable and sustainable electrodes and electrolytes with high capacity and longevity are increasingly sought after to meet the demand for a fast-charging EV with long mileage and exceptional safety. Leading battery technologies include alkali ion, alkaline ion, and transition metal ion types wherein the redox reaction is accompanied by intercalation of metal ions into the crystal structure of cathode, which typically facilitates a high voltage potential across the cell, resulting in excellent energy density. On the other hand, the theoretical energy density C_t given below is limited by the amount of electrons n per mole of electrode M participating in the redox reaction, which is around 250mAh/g for intercalating lithium-ion batteries, and dependent upon the composition of cathode material. [3]

$$C_t = \frac{nF}{3.6M} \tag{1}$$

Due to incomplete lithiation/delithiation in the cathode, the energy density of lithium-ion batteries is at a fraction of their corresponding theoretical capacity. Figure 3 illustrates an overview of the real cycling performance for various cathode materials currently pursued in lithium-ion battery as an initiative from U.S. department of energy to reduce reliance on cobalt, which is an expensive and unsustainable component to source.[4] Evidently, capacity degradation is a troublesome factor present in all cathodes, which leaves ample opportunity for material research in a stable and robust electrode capable of resolving the issue of limited longevity.

Compositional complex or high entropy material system is one area in which incorporation of multiple components is expected to considerably reduce the overall system free energy, thereby imparting potential electrodes with exceptional structural stability for prolonged electrochemical cycles. The idea of high entropy systems pioneered by Yeh set the stage for almost twenty years of research into combining multiple primary material components into a system whose behavior supersedes simpler binary or ternary systems of the same components. [5] The seminal work in high entropy metallic alloys showed formation of modulated solid solutions with nanocrystalline precipitations insofar as inter granular dislocations are impeded to result in excellent mechanical strength when compared to ternary Ti-6Al-4V, for example.[5]

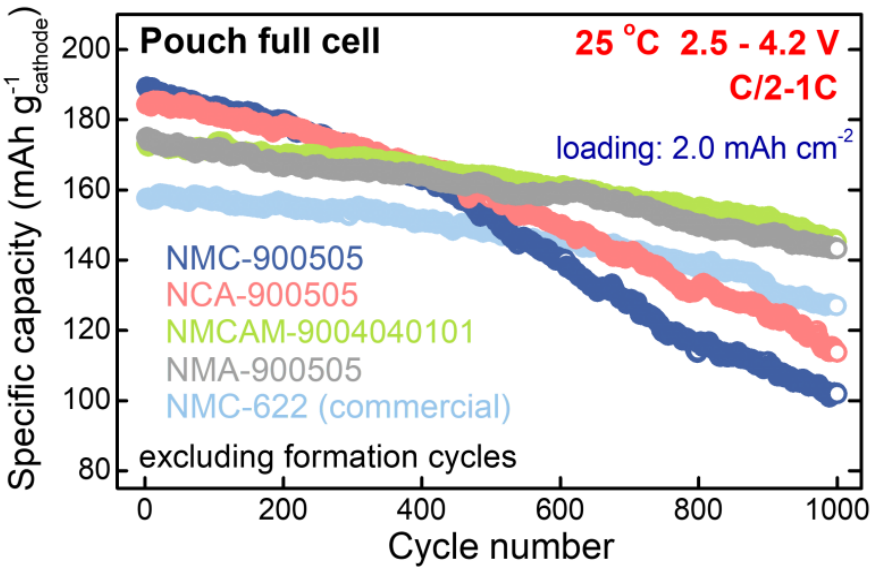

Figure 3 Electrochemical cycling performance of various lithium-ion cathodes at low or zero cobalt content with nickel manganese cobalt (NMC) 622 as the baseline. [4]

The stabilization mechanism in high entropy materials is theorized to be governed by configurational entropy, whose contribution to the free energy of the system at sufficiently high temperature becomes predominate over enthalpy of mixing as the number of components N is increased, as given in equations below,

$$S = -k_B \sum_{i=1}^{N} x_i \ln x_i \quad (2)$$

where the maximum configurational entropy is achieved when system components are equimolar ($x_i = 1/N$),

$$S = k_B \ln N \quad (3)$$

the effects of which is illustrated in Figure 4. It is worth noting however, entropy alone does not always dictate the material system, Hume Rothery rules and system components, as numerous published quinary systems have shown, also influence system outcome to some extent, corroborating strong evidence of not only structure-property but also of composition-property correspondences. [5, 6, 7, 8, 9, 10]

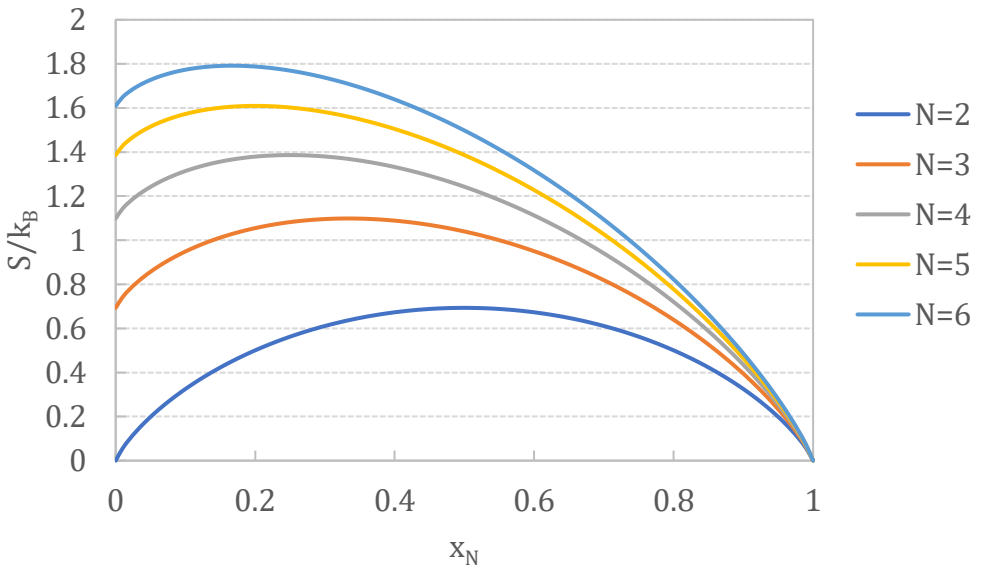

Figure 4 Entropy stabilized system with respect to k_B as a function of the mole fraction of incorporated components x_N where N stands for the number of components.

Discoveries of serendipitous properties in high entropy metallic alloys motivated similar research into ceramic materials wherein effects pertaining to electronic, magnetic, thermal, and optical properties are being probed to establish a fundamental understanding in this growing field. [11] Compositional complex oxides (CCO), as a result, are synthesized and studied increasingly to validate their properties and potential applications so as to develop novel material theories and bring advanced material solutions across the research community at large. Among various crystal structures successfully synthesized in high entropy oxides, rocksalt and spinel in particular, because their capacity to accommodate ion exchange, are promising candidates for energy storage. When subjected to electrochemical cycling reactions, robust 3D structure in spinel crystals hold lower site energy, which lead to potential plateaus, whereas rocksalt and layered structures tend to distort and thereby hold higher site energy, which gives rise to potential sloping. [12] Moreover, high entropy oxides tend to form disordered solid solution, if the system is entropy stabilized, which would normally be detrimental to ion diffusion due to

reduced inter atomic spacing, [13, 14, 15] yet reports of remarkable ionic conductivity > 10^{-3} S cm^{-1} in lithium-ion batteries demonstrate disorder can be conducive ion diffusion. [11, 16] One proposed underlying mechanism to support improved diffusion in disordered crystals is a facile network for octahedral to octahedral hopping via intermediate tetrahedral space, which is facilitated by low electrostatic repulsions stemming from having an excess ($x \geq \sim 1.1$) exchange ion of interest. [15, 17, 18]

Combining multi-valent transitional metals such as vanadium and manganese can promote exchange of multiple electrons during redox cycles, which can yield a higher energy density compared to monovalent or divalent species, an area increasingly attempted in battery research to improve storage capacity, though the capacity gain is often offset by reduced crystal field stabilization, which results in a wider potential drop and reduced storage longevity. [19, 20] Presented in this paper is an attempt to stabilize a novel multi-valent transition metal oxide by entropy with the expectation it may improve storage longevity, the results of which reported below allude to a conversion type reaction with terrific capacity and longevity upwards of 700mAh/g and 100 cycles, respectively, at 0.5A/g. The findings suggest entropy is a probable contribution to cycling stability while composition and material structure facilitated the reaction mechanism and the capacity. Additional trial and error are necessary to elucidate a more in depth understanding of the exact material underpinnings.

2. Experimental

Solid state synthesis, nebulized spray pyrolysis, flame spray pyrolysis, and reverse co-precipitation are primary pathways for synthesizing high entropy oxide, each of which produces unique particle morphology and size, and all of which yield similar system, making method selection a matter of accessibility. Reverse co-precipitation shown in Figure 5 below was selected from a safe and facile lab operation point of view, which required precise control of pH whereby a precursor solution dissolved from equimolar high purity transition metal salt of $VOSO_4 \cdot (H_2O)_x$ ($3 \leq x \leq 5$), $MnSO_4 \cdot H_2O$, $Fe(NO_3)_3 \cdot 9H_2O$, $Co(NO_3)_2 \cdot 6H_2O$, and $Ni(NO_3)_2 \cdot 6H_2O$ is slowly co-precipitated. The amorphous precipitation is then separated from the mixture, dried, and subsequently calcined at 900°C to obtain a fine crystalline powder. pH, rate of precipitation as well as calcination temperature are parameters controlled to dictate the phase, size, and morphology of the synthesized material. [21]

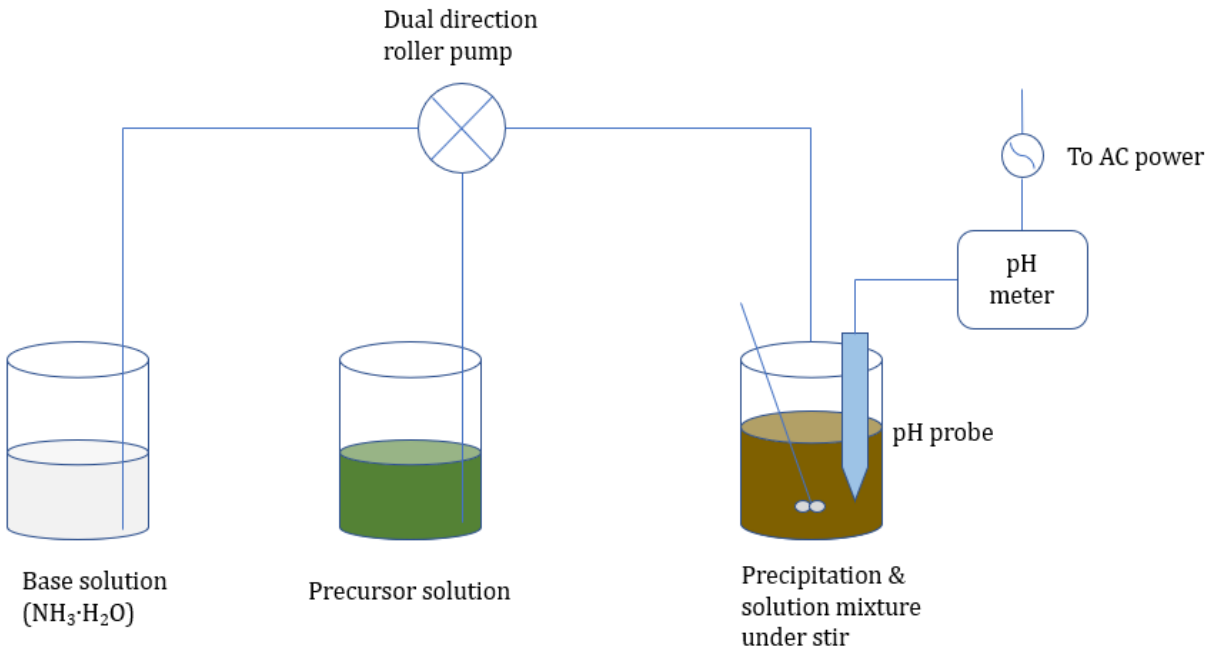

Figure 5 Schematic of reverse co-precipitation synthesis showing the precursor solution of predetermined flow rate is pumped into the base solution to the right in which the equimolar transition metal ions contained are co-precipitated. Note the base solution on the left is used as auxiliary to maintain a pH threshold until the precursor solution is completely co-precipitated.

Electrode was prepared by mixing solids of synthesized oxide material, carbon black, and polyvinylidene fluoride (PVDF) at a ratio of 7:2:1 and dispersing the mixture in appropriate amount of *N*-Methyl-2-pyrrolidone (NMP). The slurry mixture was cast onto a copper substrate and dried at 80 °C. Areal load of the active material was 0.5-1 mg/cm^2. CR2032 coil cell batteries were assembled in Ar filled glove box with lithium foil, 1M $LiPF_6$ in 1:1 ethylene carbonate and diethyl carbonate by volume, and glass microporous film as counter electrode, electrolyte, and separator, respectively. The energy density obtained is based on the load of active material.

Crystallographic information of the synthesized powder material was acquired from Bruker D8 Discover Microfocus X-ray diffractometer (XRD), with a Cu Kα x-ray source of 50kV and 1000μA, a 0.5mm collimator, and a Pilatus3 R 100K-A detector, the results of which were characterized using Diffract.EVA software and database.

Microstructural imaging and composition were measured on JEOL JSM-6010Plus scanning electron microscope (SEM) with integrated energy dispersive X-ray spectrometer (EDS) and software analysis package.

All X-ray photoelectron spectroscopy (XPS) spectra were taken on a Kratos Axis-Ultra DLD spectrometer using the electrostatic lens. This instrument has a monochromatized Al Kα X-ray and a low energy electron flood gun for charge neutralization. X-ray spot size for these acquisitions was on the order of 700 x300 μm. Pressure in the analytical chamber during spectral acquisition was less than 1 x 10-8 Torr. Pass energy for survey spectra (composition) was 160 eV. Pass energy for the high resolution spectra was 40 eV. The take-off angle (the angle between the sample normal and the input axis of the energy analyzer) was 0º (0 degree take-off angle ~ 100 Å sampling depth). The Kratos Vision2 software program was used to determine peak areas and to calculate the elemental compositions from peak areas. CasaXPS was used to peak fit the high resolution spectra. For the high-resolution spectra, a Shirley background was used and all binding energies were referenced to the C ls C-C bonds at 285.0 eV.

Galvanostatic charge/discharge measurements were obtained from Neware battery test system. Cyclic voltammetry and electrochemical impedance spectroscopy were measured on Solartron. All electrochemical tests were carried out at room temperature.

3. Results and discussion

Figure 6 shows the as prepared compositional complex oxide is consisted of a primary spinel phase and a secondary triclinic phase, suggesting entropy stabilization at 900 °C was insufficient to overcome the enthalpy of mixing in this particular system, and higher calcination temperature of 1000 °C caused the loose powder to sinter and yielded a solid chunk, thereby rendering it ineffectual. Nonetheless, the primary spinel phase entails a conducive crystal structure for ion exchange and is expected to facilitate the redox lithiation/delithiation cycles. Moreover, compared to binary spinel like $LiMn_2O_4$, which is prone to potential drop originating from a cubic to tetragonal phase transformation as the lithium ion is increasingly incorporated into the crystal, [22, 23] entropic contribution in the CCO may be sufficient to impart enhanced structural stability insofar as charge storage longevity can be significantly improved.

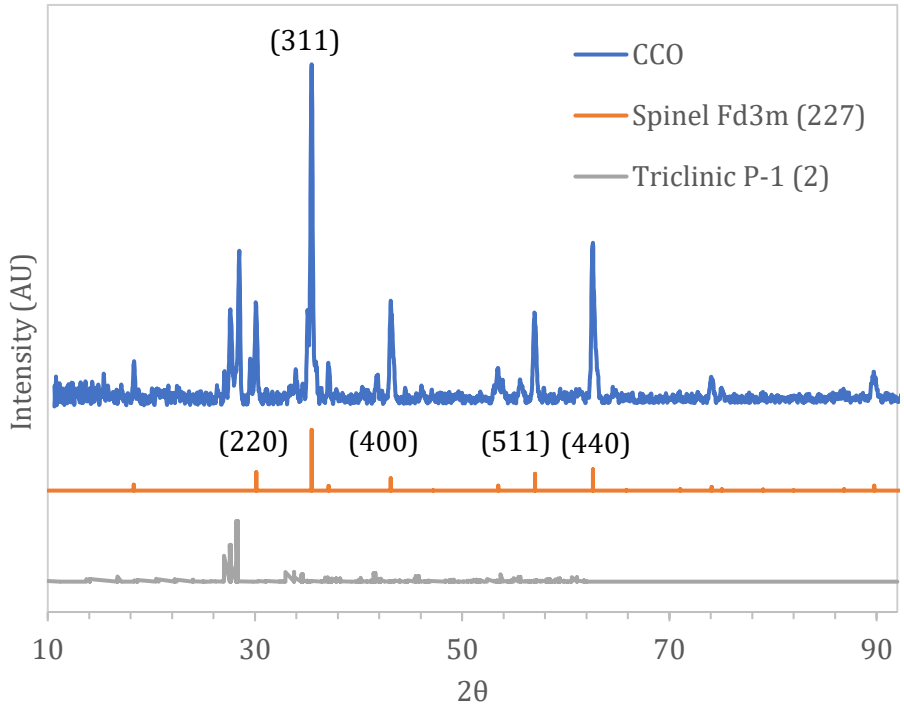

Figure 6 XRD pattern of synthesized compositional complex oxide (CCO) and reference phases.

To confirm the composition the as synthesized CCO powder was measured by SEM and cross referenced with XPS. Figure 7 shows the grain size of the CCO is predominantly in the nanometer regime, and uniform elemental distribution is observed. The absence of nickel is attributed to the formation of ammonium nickel complex during co-precipitation. [24] Quantitatively, the composition of the CCO is given in atomic % in Table 1, which shows a mean ratio of 1:0.96:1.38:1.10:0.10 for V, Mn, Fe, Co, and Ni, respectively, hereby approximated as near equimolar sans nickel. Deviations from EDS to XPS may be caused by a combination of operator error, equipment error, as well as intrinsic uncertainties from each technique, such as overlapping of Auger peaks in XPS.

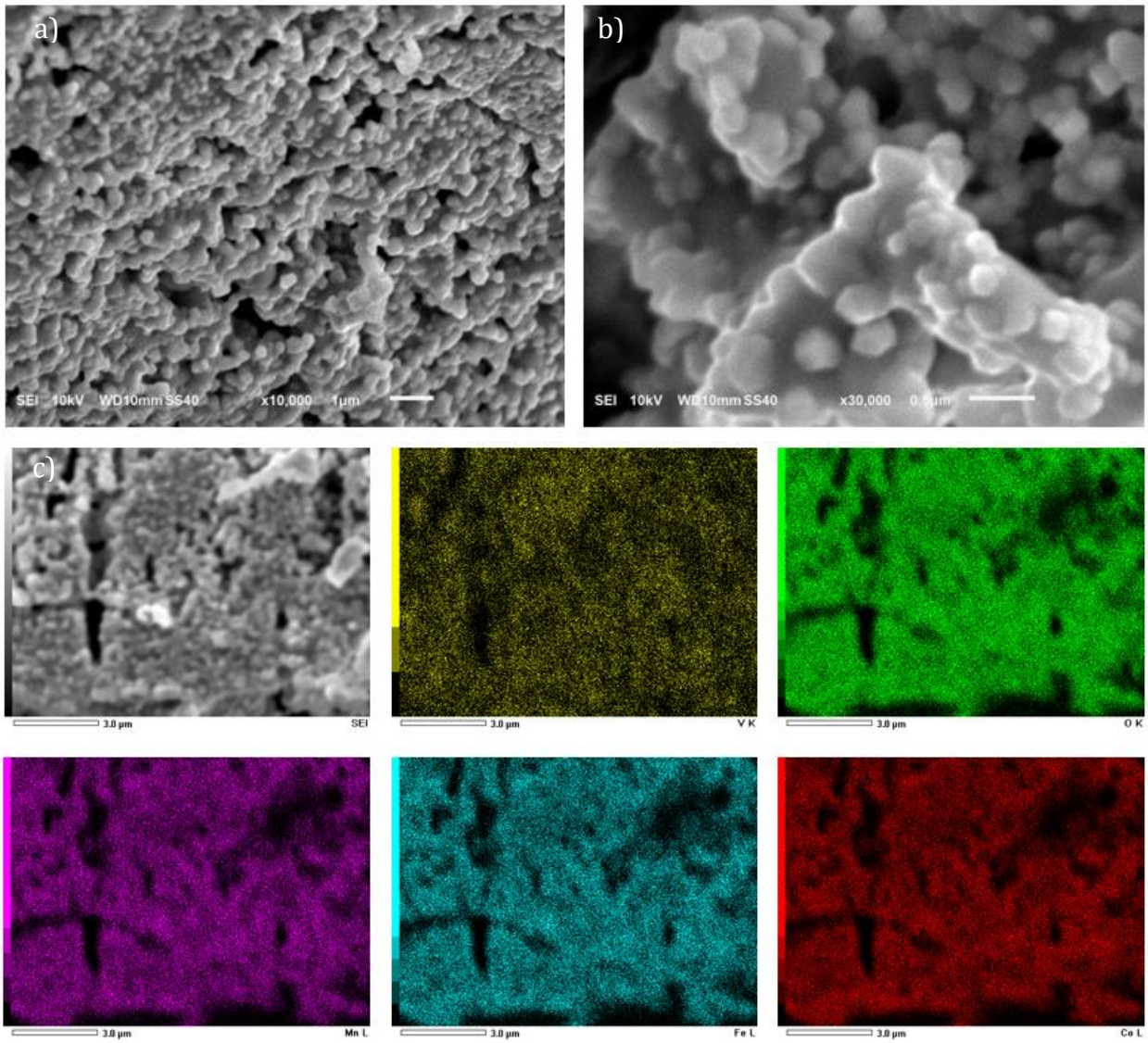

Figure 7 SEM of as synthesized CCO powder at a) 10,000 magnification and b) 30,000 magnification both shown predominantly nanometer sized grains. EDS data c) indicate uniform elemental distribution on the corresponding scale.

	V	Mn	Fe	Co	Ni	O
EDS	11.48	8.75	13.32	8.96	-	44.72
XPS	6.07	6.97	9.69	8.64	1.16	42.76

Table 1 Quantitative data of CCO composition in atomic % by EDS and XPS. Minor impurities e.g., C, Si, are not accounted for.

Oxidation states of composed transition metals in the CCO were measured by XPS to elucidate the formula unit, the results of which are shown in Figure 8. Nickel had a low signal to noise ratio due to its trace presence, so it was unable to be resolved with confidence, though the deconvoluted Ni $2p_{3/2}$ multiplets at around 855 eV points to Ni^{2+}. [25] Cobalt deconvolution was indicative of both Co^{2+} and Co^{3+}, with negligible Co^{2+} peak shown in light orange at around 786 eV, suggesting Co^{3+} was the primary oxidation state. Similarly, iron was present in both trace Fe^{2+} and predominant Fe^{3+}, and trace Fe^{2+} can be attributed to overlapping of Augers with Ni, Co as well as surface exposure to air. [26, 27] Manganese was resolved as Mn^{3+} from its characteristic $2p_{3/2}$ peak at around 642 eV, again trace Mn^{2+} may be inferred from the miniscule satellite peak of MnO at around 647 eV. [25] Vanadium was determined to be V^{5+} at its distinctive $2p_{3/2}$ and $2p_{1/2}$ peaks around 518 eV and 524 eV, respectively. [28]

The multi-valent oxidation states rendered deconvolution of the formula unit null. As such, a generic formula unit of (VMnFeCo)O is proposed based on the composition gathered from EDS/XPS and the presumption of Ni being a trace and lesser component. The fractions of each transition metal component are dictated by their respective oxidation state, and the collective transition metal ligand carries a positive two charge by electroneutrality. More accurate depiction of the formula unit such as $(V_{0.25}Mn_{0.25}Fe_{0.25}Co_{0.25})_{1-x}Ni_xO$ accounting the lesser Ni content may be necessary to promote fundamental understandings of the system.

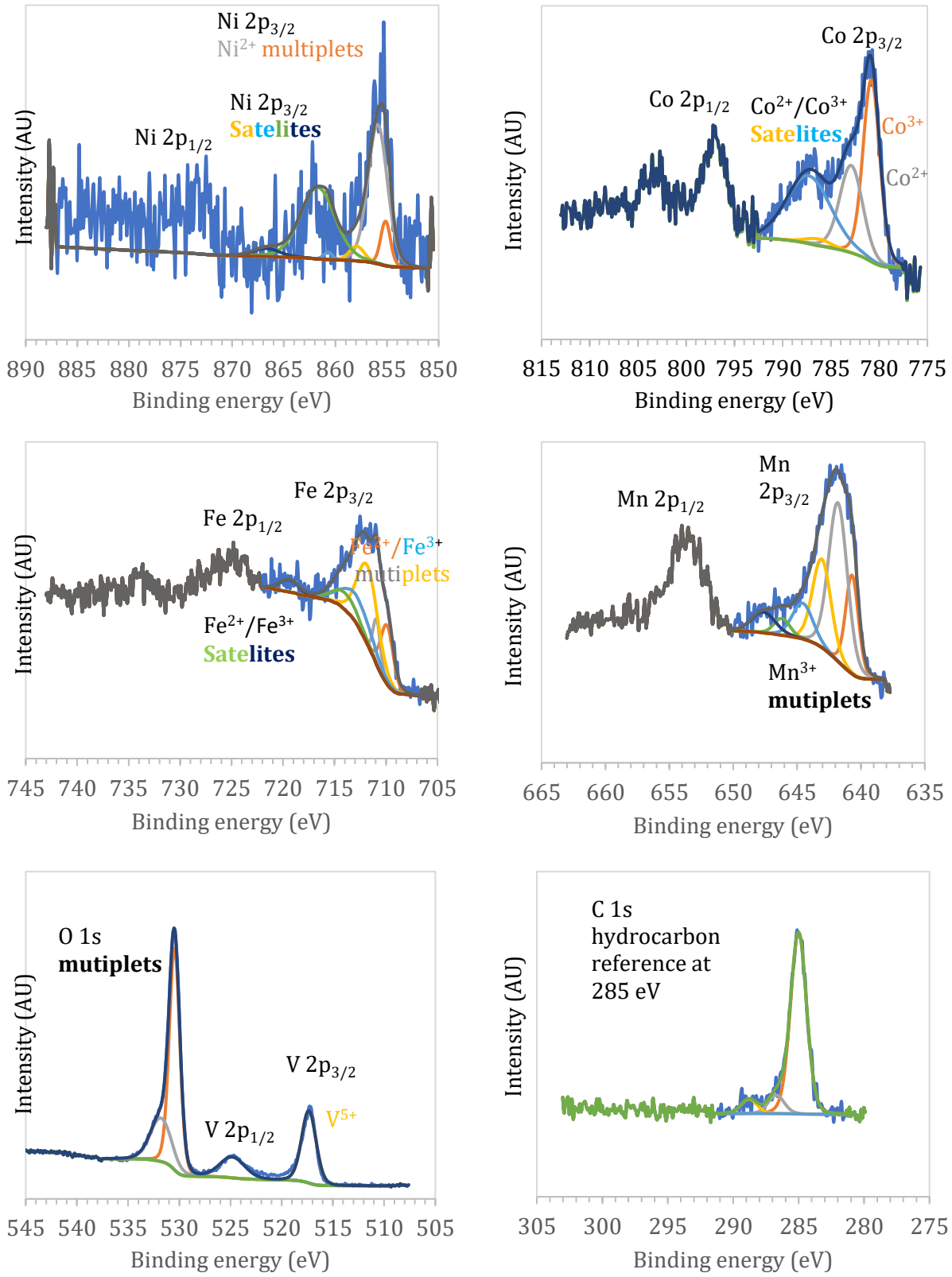

Figure 8 XPS of the as prepared CCO powder with spectra of individual transition metals at their respective oxidation state.

Cyclic voltammogram at scan rate of 0.1mV/s shown in Figure 9 indicates the initial strong irreversible anodic peak at approximately 0.45V was associated with reduction of transition metal ions and formation of solid electrolyte interface (SEI). [31] Interestingly, peak shift and multiple reversible anodic peaks showed up in the following cycles, which can be attributed to nonuniform reduction of transition metals to discrete states. Cathodic peaks corresponding to oxidation of the reduced transition metals species remained steady at around 1.3V and 1.7V, which corroborates the overall electrochemical cell was reversible. As expected, increased scan rate led to thinning of the diffusion layer, which manifested in larger current responses, suggesting the electrode was stable and robust, thereby conducive to storage longevity. [32, 33]

To probe the mechanism of the pertaining redox reactions, logarithmic correlations of peak current *i* vs scan rate *v* is plotted according to equations below,

$$i = av^b \tag{4}$$

$$\log(i) = blog(v) + \log(a) \tag{5}$$

where b=0.5 and b=1.0 correspond to wholly diffusion controlled and kinetic controlled reactions, respectively. [29, 30, 34] Based on b values obtained in Figure 9, reduction of the transition metals was deemed concurrently governed by long range diffusion and short range surface kinetics, which meant surface reaction was as fast as long range ion diffusion, whereas the oxidation reactions were more influenced by slower long range diffusion. The findings make sense insofar as oxidation of transition metals in the CCO electrode was limited by the rate of lithium metal diffusion to the counter electrode while diffusion of lithium ion during reduction was facile. Thus, the reaction mechanism was more akin to conversion type as opposed to

intercalation type, which normally has a slower surface kinetic (b>0.75) as a result of low electrostatic energy at ion intercalating sites.

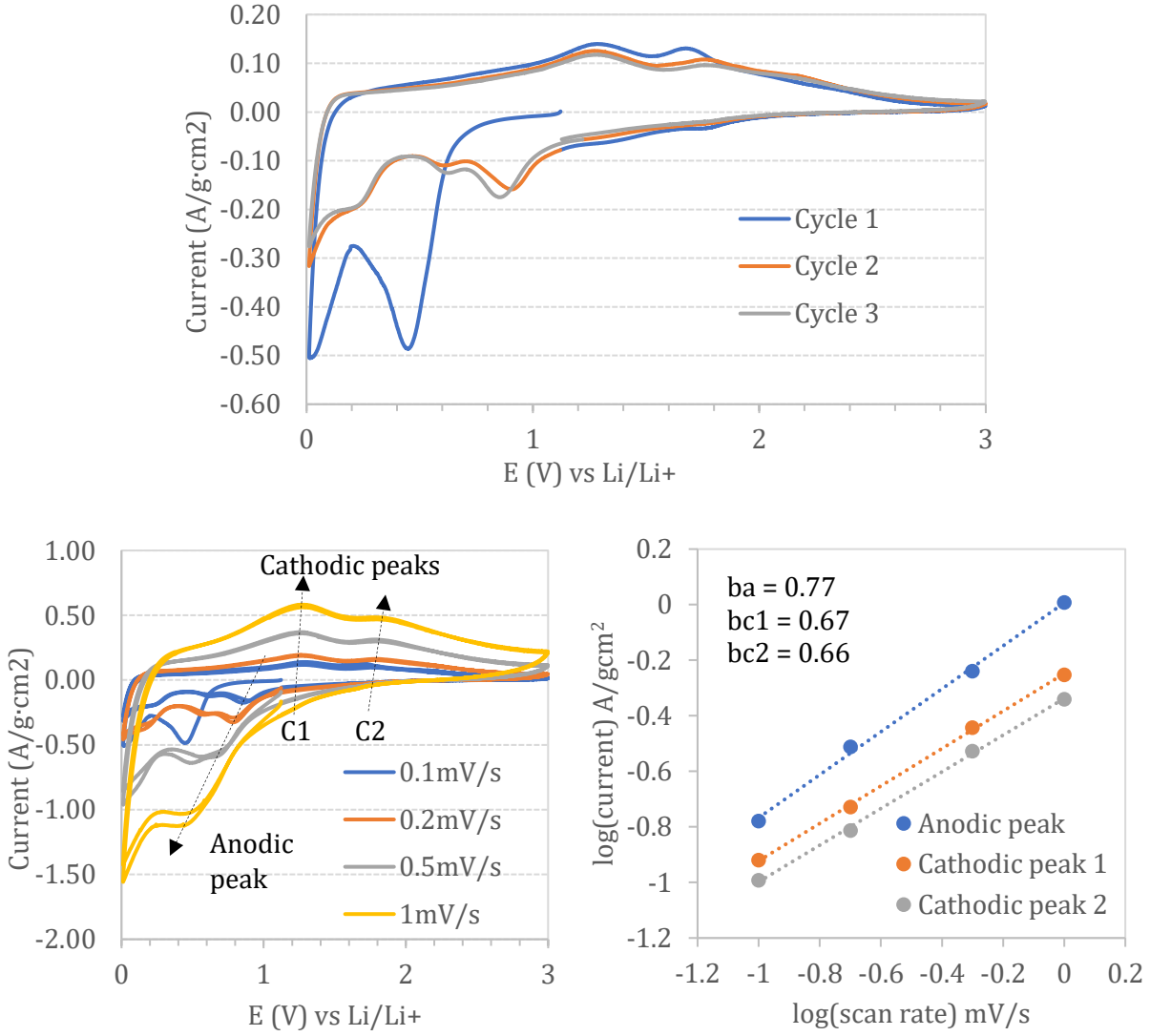

Figure 9 Cyclic voltammetry of the assembled CCO battery measured at 0.1 mV/s (top), and various scan rates (bottom left). A single anodic peak and two cathodic peaks C1, C2 were identified and characterized by power law correlation between scan rate and current. Anodic ba and cathodic bc power exponents obtained suggest the reaction was both kinetic and diffusion controlled.

Galvanostatic data in Figure 10 provides more evidence for supporting a conversion reaction storage mechanism because of the superior capacity the electrochemical system entailed. Furthermore, analogous electrodes by ion intercalation, due to their limited number of ion exchanging tetrahedral and octahedral sites, would normally see only about half of their theoretical capacity measured empirically. Initial capacity attenuation is another common trend in conversation reaction resulting from partial irreversibility of higher oxidation states, e.g., reduced Co^{3+} in the initial cycle to Co metal would only oxidize to Co^{2+} in the following cycles. [31, 37] The voltage profiles in Figure 10c also typified that of conversion reaction and shown nearly linear sloping after the first discharge cycle, after which the CCO would nucleate into nanoscale crystals only detectable by transmission electron microscopy (TEM). [7, 35, 36]

Capacity growth at the onset of about 25 cycles in Figure 10a can be attributed to pulverization of the CCO particles whereby increased particle surface area promoted higher charge storage density, which is another characteristic of conversion reaction, and a major driver for high Coulombic efficiency. [38] High Coulombic efficiency and cycling stability evident in Figure 10 (a, c, d) however, are atypical in binary or ternary conversion type oxides, particularly when they are not modified to favorable morphology and size. [39, 40] Thus, entropic stabilization is considered a probable contribution for enhanced storage longevity in the CCO. Moreover, capacity discrepancy from the corresponding amorphous CCO in Figure 10b is indicative of entropy stabilization as a facilitator for not only storage longevity, but also storage capacity. It is worth noting the initial discharge plateau at approximately 0.6V alludes to the potential of engineering an intercalation type anode, because a large sloping voltage window is typically not feasible in battery applications. Largely reversible rate responses in Figure 10c suggest both electrodes were preserved, which is impressive considering increased current

density often lead to build up of anodic deformation and rapid cell degradation in commercial lithium metal batteries. [41] Capacity drops in Figure 10c at increased current densities is driven by their equivalent faster kinetics, which rendered the redox reactions diffusion limited, thereby reducing the total amount of participating Li/Li^+ couple per cycle.

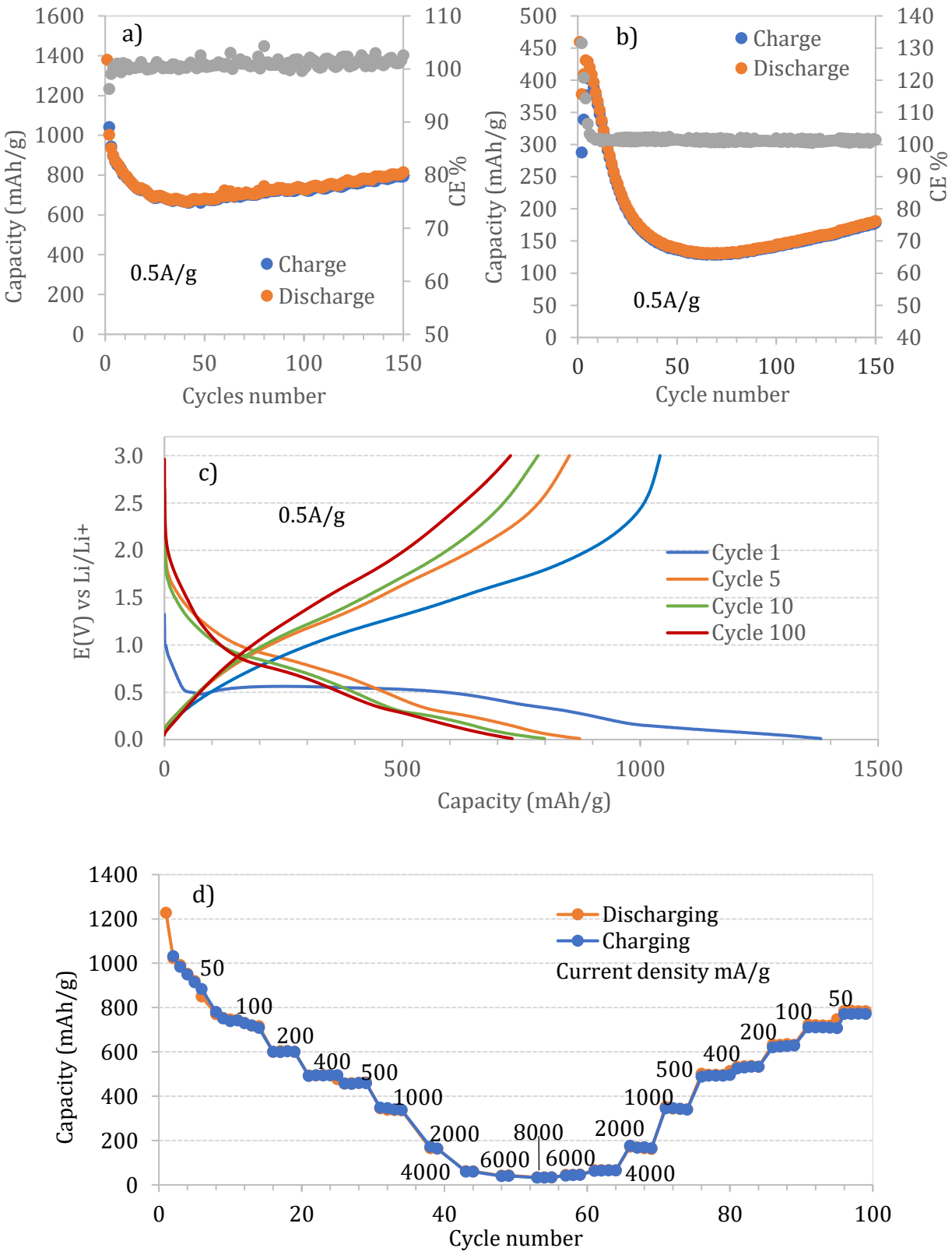

Figure 10 Galvanostatic charge/discharge responses of the calcined CCO (a, c, d) and the corresponding amorphous CCO b) at a preset of current densities and cycles.

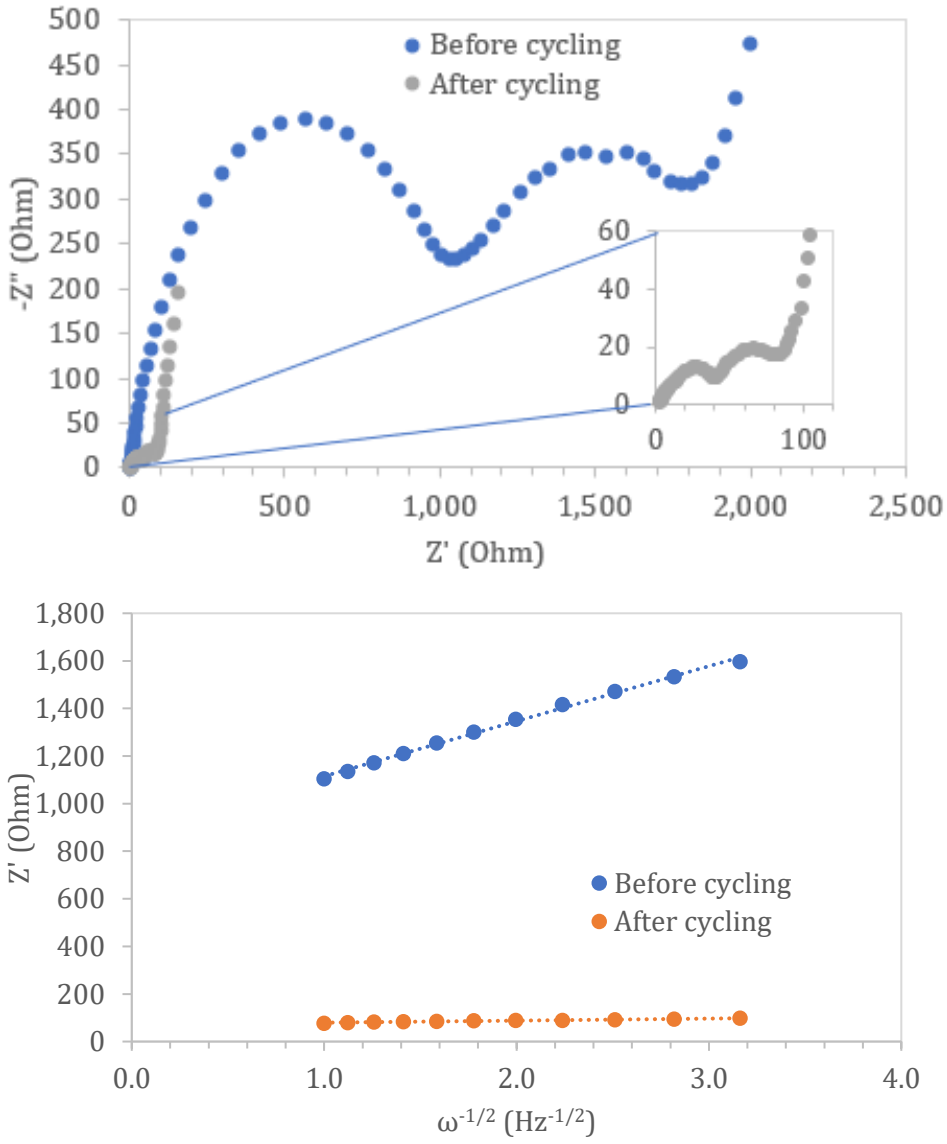

Figure 11 Nyquist electrochemical impedance spectra of as prepared and post CV swept Li-CCO cell (top), and impedance responses at low frequencies of 0.1-1.0 Hz. (Cross reference Figure 9)

Figure 11 is telling of an intermediate SEI layer R_{SEI} in addition to bulk solution R_s, charge transfer R_{Ct}, and Warburg diffusional W layers. Their combined effects given by equations below are employed to estimate the diffusion coefficient of lithium ions D_{Li} in the redox reaction, [42, 43]

$$D_{Li} = \frac{R^2T^2}{2A^2n^4F^4C^2\sigma^2} \quad (6)$$

$$Z' = \sigma\omega^{-\frac{1}{2}} + R_S + R_{SEI} + R_{Ct} \quad (7)$$

where R is the gas constant, T is the measurement temperature in Kelvin, A is the electrode area (0.785 cm^2), n is the number of molar redox electrons, F is the Faraday constant, C is the concentration of Li^+ (1M), σ is the Warburg constant, whose correlation with impedance Z', angular frequency ω and components of cell impedance is given above.

Kinetic parameters of the CCO half cell hence obtained are given in Tables 2-4 for $2 \leqq n \leqq 4$ equivalent to approximately 700-1400 mAh/g in theoretical capacity according to equation 1, the gist of which can be substantiated by capacity measured in the prior discussion. Starting SEI impedance is a bit larger than charge transfer impedance, which can be ascribed to activation energy required to initiate the redox reaction. Both impedances reduced by more than one order of magnitude after twelve CV sweeps, attributable to particle pulverization discussed earlier. Moreover, both impedances became identical, resembling a reaction with equal contribution of surface kinetic and long range diffusion, which is consistent with the discharge cycles and the reduction of transition metal ions at b=0.77 mentioned above. Diffusion coefficients estimations after initial activation cycles are 1-2 order of magnitude higher than current commercial systems such as lithium cobalt oxide, the reason of which can be assigned to high site energy barrier present in the intercalation electrodes. Finally, one can expect the CCO to become increasingly diffusion limited as a greater number of electrons start participating in the conversion reaction, a characteristic confirmed again from Tables 2-4.

n=2	R_S [Ω]	R_{SEI} [Ω]	R_{Ct} [Ω]	σ_W [$\Omega Hz^{1/2}$]	D_{Li+} [cm^2/s]
Before	2.9	1160	990	231.3	6.72E-14
After	3.3	50	50	8.5	4.98E-11

Table 2 Kinetic parameters of the CCO with the number of redox electrons n presumed 2.

n=3	R_S [Ω]	R_{SEI} [Ω]	R_{Ct} [Ω]	σ_W [$\Omega Hz^{1/2}$]	D_{Li+} [cm^2/s]
Before	2.9	1160	990	231.3	1.33E-14
After	3.3	50	50	8.5	9.83E-12

Table 3 Kinetic parameters of the CCO with the number of redox electrons n presumed 3.

n=4	R_S [Ω]	R_{SEI} [Ω]	R_{Ct} [Ω]	σ_W [$\Omega Hz^{1/2}$]	D_{Li+} [cm^2/s]
Before	2.9	1160	990	231.3	4.20E-15
After	3.3	50	50	8.5	3.11E-12

Table 4 Kinetic parameters of the CCO with the number of redox electrons n presumed 4.

4. Summary and prospect

A novel CCO was synthesized in hopes of improving storage longevity by entropic stabilization. Structural characterization determined the CCO was a mixture of primary spinel and secondary triclinic phases, both of which contained mostly nanoscale grains with uniform distribution of transition metal components with the exception of nickel, whose disposition to form ammonium complex resulted in its trace precipitation. Composition and oxidation states of the CCO revealed a near equimolar and multi-valent formula unit of $(V_{0.25}Mn_{0.25}Fe_{0.25}Co_{0.25})_{1-x}Ni_xO$, which is synonymous with a S/k_B ratio of about 1.4, a key indicator of significant entropic contribution to phase stabilization. Cyclic voltammetry, galvanostatic and kinetic data made a strong case for an entropy stabilized conversion type reaction mechanism of the CCO half cell. By examining existing databases of analogous materials and delve deeper into finer domain of

the CCO, one can shed light on ionic, atomic, and electronic interactions involved not only in the electrochemical cell but also in potential applications, an area of growing pertinence and increasingly reliant on state of the art computation and instrumentation, e.g., artificial intelligence (AI) and scanning transmission electron microscopy (STEM), to help researchers understand material fundamentals and develop innovative solutions to meet many challenges faced in the broader community today. Further CCO research therefore, may lead to resolutions to capacity, longevity constraints in current energy storage systems, and pave the way for a more sustainable energy cycle.

References

1. U.S. Energy Information Administration, “Monthly Energy Review”, April 2021, preliminary data for 2020.
2. Bloomberg New Energy Finance, “Electric Vehicle Outlook 2020,” BloombergNEF, New York, 2020.
3. Zhi, Mingjia, et al. "Nanostructured carbon–metal oxide composite electrodes for supercapacitors: a review." *Nanoscale* 5.1 (2013): 72-88.
4. U.S. Department of Energy Vehicle Technologies Office,” Reducing Reliance on Cobalt for Lithium-ion Batteries”, April 2021
5. Yeh, J-W., et al. "Nanostructured high-entropy alloys with multiple principal elements: novel alloy design concepts and outcomes." *Advanced engineering materials* 6.5 (2004): 299-303.
6. Rost, Christina M., et al. "Entropy-stabilized oxides." *Nature communications* 6.1 (2015): 1-8.
7. Sarkar, Abhishek, et al. "High-entropy oxides: fundamental aspects and electrochemical properties." *Advanced Materials* 31.26 (2019): 1806236.
8. Otto, Frederik, et al. "Relative effects of enthalpy and entropy on the phase stability of equiatomic high-entropy alloys." *Acta Materialia* 61.7 (2013): 2628-2638.
9. Sarkar, Abhishek, et al. "Rare earth and transition metal based entropy stabilised perovskite type oxides." *Journal of the European Ceramic Society* 38.5 (2018): 2318-2327.
10. Djenadic, Ruzica, et al. "Multicomponent equiatomic rare earth oxides." *Materials Research Letters* 5.2 (2017): 102-109.
11. Musicó, Brianna L., et al. "The emergent field of high entropy oxides: Design, prospects, challenges, and opportunities for tailoring material properties." *APL Materials* 8.4 (2020): 040912.
12. Liu, Chaofeng, Zachary G. Neale, and Guozhong Cao. "Understanding electrochemical potentials of cathode materials in rechargeable batteries." *Materials Today* 19.2 (2016): 109-123.
13. Kang, Kisuk, et al. "Electrodes with high power and high capacity for rechargeable lithium batteries." *Science* 311.5763 (2006): 977-980.
14. Rougier, A., P. Gravereau, and C. Delmas. "Optimization of the composition of the Li1− z Ni1+ z O 2 electrode materials: structural, magnetic, and electrochemical studies." *Journal of The Electrochemical Society* 143.4 (1996): 1168.
15. Kang, Kisuk, and Gerbrand Ceder. "Factors that affect Li mobility in layered lithium transition metal oxides." *Physical Review B* 74.9 (2006): 094105.
16. Bérardan, D., et al. "Room temperature lithium superionic conductivity in high entropy oxides." *Journal of Materials Chemistry A* 4.24 (2016): 9536-9541.
17. Lee, Jinhyuk, et al. "Unlocking the potential of cation-disordered oxides for rechargeable lithium batteries." *science* 343.6170 (2014): 519-522.
18. Van der Ven, A., and G. Ceder. "Lithium diffusion in layered Li x CoO2." *Electrochemical and Solid-State Letters* 3.7 (2000): 301.

19. Armstrong, A. Robert, and Peter G. Bruce. "Synthesis of layered LiMnO2 as an electrode for rechargeable lithium batteries." *Nature* 381.6582 (1996): 499-500.
20. De Picciotto, L. A., et al. "Structural characterization of delithiated LiVO2." *Materials research bulletin* 19.11 (1984): 1497-1506.
21. Sarkar, Abhishek, et al. "Nanocrystalline multicomponent entropy stabilised transition metal oxides." *Journal of the European Ceramic Society* 37.2 (2017): 747-754.
22. Park, Jung-Ki, ed. *Principles and applications of lithium secondary batteries*. John Wiley & Sons, 2012.
23. Nazri, Gholam-Abbas, and Gianfranco Pistoia, eds. *Lithium batteries: science and technology*. Springer Science & Business Media, 2008.
24. Biesuz, Mattia, et al. "Synthesis and sintering of (Mg, Co, Ni, Cu, Zn) O entropy-stabilized oxides obtained by wet chemical methods." *Journal of materials science* 53.11 (2018): 8074-8085.
25. Nunney, Tim. "XPS Reference Table of Elements for Mining and Minerals", Thermal Fisher Scientific, June 2020.
26. Grosvenor, A. P., et al. "Investigation of multiplet splitting of Fe 2p XPS spectra and bonding in iron compounds." *Surface and Interface Analysis: An International Journal devoted to the development and application of techniques for the analysis of surfaces, interfaces and thin films* 36.12 (2004): 1564-1574.
27. Biesinger, Mark C., et al. "Resolving surface chemical states in XPS analysis of first row transition metals, oxides and hydroxides: Cr, Mn, Fe, Co and Ni." *Applied Surface Science* 257.7 (2011): 2717-2730.
28. Ghimbeu, Camelia Matei, et al. "Vanadium nitride/carbon nanotube nanocomposites as electrodes for supercapacitors." *Journal of Materials Chemistry* 21.35 (2011): 13268-13275.
29. Augustyn, Veronica, Patrice Simon, and Bruce Dunn. "Pseudocapacitive oxide materials for high-rate electrochemical energy storage." *Energy & Environmental Science* 7.5 (2014): 1597-1614.
30. Wang, John, et al. "Pseudocapacitive contributions to electrochemical energy storage in TiO2 (anatase) nanoparticles." *The Journal of Physical Chemistry C* 111.40 (2007): 14925-14931.
31. Cao, Kangzhe, et al. "Recent progress in conversion reaction metal oxide anodes for Li-ion batteries." *Materials Chemistry Frontiers* 1.11 (2017): 2213-2242.
32. Allen, L. R. F., and J. Bard. "Electrochemical Methods Fundamental and Applications., John Wiley&Sons." *Inc., The United State of America* (2001).
33. Savéant, Jean-Michel. *Elements of molecular and biomolecular electrochemistry: an electrochemical approach to electron transfer chemistry*. John Wiley & Sons, 2006.
34. Shen, Laifa, et al. "Peapod-like Li3VO4/N-doped carbon nanowires with pseudocapacitive properties as advanced materials for high-energy lithium-ion capacitors." *Advanced Materials* 29.27 (2017): 1700142.
35. Sarkar, Abhishek, et al. "High entropy oxides for reversible energy storage." *Nature communications* 9.1 (2018): 1-9.

36. Qiu, Nan, et al. "A high entropy oxide (Mg0. 2Co0. 2Ni0. 2Cu0. 2Zn0. 2O) with superior lithium storage performance." *Journal of Alloys and Compounds* 777 (2019): 767-774.
37. Luo, Langli, et al. "Atomic resolution study of reversible conversion reaction in metal oxide electrodes for lithium-ion battery." *Acs Nano* 8.11 (2014): 11560-11566.
38. Poizot, P. L. S. G., et al. "Nano-sized transition-metal oxides as negative-electrode materials for lithium-ion batteries." *Nature* 407.6803 (2000): 496-499.
39. Goriparti, Subrahmanyam, et al. "Review on recent progress of nanostructured anode materials for Li-ion batteries." *Journal of power sources* 257 (2014): 421-443.
40. Ji, Liwen, et al. "Recent developments in nanostructured anode materials for rechargeable lithium-ion batteries." *Energy & Environmental Science* 4.8 (2011): 2682-2699.
41. Jiao, Shuhong, et al. "Behavior of lithium metal anodes under various capacity utilization and high current density in lithium metal batteries." *Joule* 2.1 (2018): 110-124.
42. Takami, Norio, et al. "Structural and kinetic characterization of lithium intercalation into carbon anodes for secondary lithium batteries." *Journal of The Electrochemical Society* 142.2 (1995): 371.
43. Chou, Shu-Lei, et al. "Rapid synthesis of Li4Ti5O12 microspheres as anode materials and its binder effect for lithium-ion battery." *The Journal of Physical Chemistry C* 115.32 (2011): 16220-16227.